Available online at www.sciencedirect.com

SCIENCE DIRECT

VIROLOGY

Virology 349 (2006) 254–263

www.elsevier.com/locate/yviro

Rapid Communication

Survival of parvovirus B19-infected cells by cellular autophagy

Akitoshi Nakashima [a,d], Nobuyuki Tanaka [a,*], Keiichi Tamai [a], Masanao Kyuuma [a], Yoshinori Ishikawa [a], Hiroyuki Sato [b], Tamotsu Yoshimori [c], Shigeru Saito [d], Kazuo Sugamura [a]

[a] *Department of Microbiology and Immunology, Tohoku University Graduate School of Medicine, 2-1 Seiryo-machi, Aoba-ku, Sendai 980-8575, Japan*
[b] *Fukuoka Red Cross Blood Center, Fukuoka 818-8588, Japan*
[c] *Department of Cell Genetics, National Institute of Genetics, Mishima 411-8540, Japan*
[d] *Department of Obstetrics and Gynecology, Toyama Medical and Pharmaceutical University School of Medicine, 2630 Sugitani, Toyama 930-0194, Japan*

Received 30 November 2005; returned to author for revision 26 January 2006; accepted 21 March 2006
Available online 27 April 2006

Abstract

Human parvovirus B19 (B19) is a well-known pathogenic agent which causes apoptosis in erythrocyte lineage cells. Here, we provide the first evidence that mitochondrial autophagy is specifically found in the B19-infected cells. The protein expression ratio for LC3-II/LC3-I increased significantly in infected cells, indicating possible involvement of cellular autophagy in the infection process. Immunofluorescence confocal microscopy analyses revealed that B19 infection induced an intracellular autophagosome as judged by endogenous LC3 staining. Moreover, inhibition of autophagy by 3-MA significantly facilitated B19-infection-mediated cell death. These results suggest a novel mechanism by which B19-infected cells survive by cellular autophagy.

Keywords: Parvovirus B19; Autophagy; LC3; 3-MA

Introduction

Cellular homeostasis is controlled by a balance of protein biosynthesis and degradation. Eukaryotic cells utilize at least two distinct pathways to degrade intracellular proteins, namely ubiquitin/proteasome- and lysosome-dependent degradation. Accumulating evidences suggest that most short-lived proteins are tagged with polyubiquitin chains and destined to be degraded by proteasomes, whereas those with relatively longer half-lives are sorted into intracellular vesicles called endosomes and lysosomes, allowing them to be digested by acid proteases. Upon exposure to various cellular stresses, including nutrient starvation and bacterial infection, the third cellular degradation system is activated that sequestrates a part of cytoplasm, organella, and pathogens. This bulk degradation system, called autophagy, is characterized as a process by which a portion of a cytoplasm including organelle gets surrounded by a so-called "isolation membrane". A small portion of cytoplasm enclosed by the de novo synthesized autophagic isolation membrane falls within the double-membrane structure, called autophagosomes. Then the vacuole membrane fuses with the lysosome, where the cytoplasm-derived materials are degraded and/or recycled.

Accumulating evidences suggest biological significance of autophagy. Although a basal level of autophagy may be routinely used to clear away intracellular proteins and organellas and is required for normal turnover of cellular components, activation of autophagy is also associated with physiological response to environmental stress. Upon nutrient starvation, for example, autophagy is required for cell survival in yeast as well as in mammals (Yoshimori, 2004). Paradoxically, upon various stresses, autophagy also plays crucial roles in programmed cell death (PCD). A caspase-independent cell death called 'Type II' programmed cell death (PCD) is characterized by an accumulation of autophagic vesicles. Further, a recent study showed that inhibition of caspase activity induces autophagy in certain cells (Yu et al., 2004), suggesting that both type I and type II PCDs may utilize autophagy. Pathogen infection is another typical 'life-threatening' stress on cells. Streptococcus pyogenes,

* Corresponding author. Fax: +81 22 717 8097.
E-mail address: n-tanaka@mail.tains.tohoku.ac.jp (N. Tanaka).

0042-6822/$ - see front matter © 2006 Elsevier Inc. All rights reserved.
doi:10.1016/j.virol.2006.03.029

known as Group A streptococcus (GAS) that invades non-phagocytic cells to escape into the cytoplasm, is eventually captured and sequestrated by autophagosomes (Nakagawa et al., 2004). In the context of intracellular pathogens, a close relationship between autophagy and some viral infection has been documented, including a double-stranded DNA virus such as herpes simplex virus 1 (HSV1) and single-stranded RNA virus species including murine hepatitis virus (MHV) and poliovirus (PV). Although autophagy is inhibited by a viral protein in HSV, it is conversely utilized for the viral replication in MHV and PV infection (Kirkegaard et al., 2004). Thus, the role of autophagy in the host seems to be dependent on each specific viral strain, but the overall relevance is still controversial.

Human parvovirus B19 is one of the smallest single-stranded DNA virus, which lacks an envelope and infects erythroid (progenitor) cells to cause several diseases including aplastic crisis in patients with hemolytic anemia, erythema infectiosum and hydrops fetalis. We and others have documented that B19 infection induces cell cycle arrest at G1 and G2/M phases, and apoptosis mediated by NS1, a non-structural protein encoded by the viral genome (Kirisako et al., 2000; Morita and Sugamura, 2002; Morita et al., 2001, 2003; Nakashima et al., 2004). Thus, apoptosis has been well documented regarding the B19-infected cells. Moreover, we have repeatedly found the enlargement of the infected cells, without a known biological significance. Here, we provide the first evidence that cellular autophagy is specifically found in the B19-infected enlarged cells and is involved in the survival of these cells.

Results

Infection of B19 parvovirus induces an FSC^{high} SSC^{high} cell population

Accumulating evidences suggest that B19 parvovirus shows cytotoxic activity against host cells including erythroid precursors (Ozawa et al., 1987; Young et al., 1984). In order to examine if the infection of B19 parvovirus induces any morphological changes on affected cells, we transduced the virus onto B19-susceptible erythroid cell line, UT7/Epo-S1. In our preliminary experiments, a morphologically distinct cell population characterized by the enlargement in cell size was observed at 48 h after the B19 virus infection (Morita et al., 2001). To further characterize the cell population, we utilized FACS analyses. When compared with mock-infected cells, a newly emerging high forward scatter (FSC) and high side scatter (SSC) cell population ($FSC^{high}SSC^{high}$; hereafter referred as population "B19-B"), was clearly visible in the B19-infected cell population (Fig. 1A). The percentages of B19-B in cell number were 34.8% and 1.8% for B19- and mock-infected cells, respectively. To determine whether the population B19-B is indeed induced by the viral infection, we checked NS1 protein expression, which is a hallmark of B19 infection. After sorting the B19-infected cells into the two distinct populations, $FSC^{med}SSC^{low}$ (hereafter referred as population "B19-A") and B19-B, cells from each population were stained with an anti-NS1 antibody. The percentages of NS1-positive cells were 28.8% and 84.6% in population of B19-A and B19-B, respectively (Fig. 1B). Since the NS1-positive cell number observed in B19-B population was significantly higher than that of the B19-A, we conclude that the B19-B population is most likely induced by the B19 infection.

Since our former study indicated that growth arrest of cells at G2 phase is highly associated with B19 infection, we examined both B19-A and B19-B populations for their cell cycle status. In the B19-infected B19-B population, cells within G2/M were 78%, as compared to 25% in B19-A, and 15% in mock-infected B19-A populations (Fig. 1C). Consistent with the clear difference observed among the three cell populations examined, cells from the B19-infected B19-B population grew significantly slower than those from the B19-A populations from B19-infected or uninfected cells (Fig. 1D). Additionally, appearance of the B19-B population was completely abrogated by the pretreatment of B19 virus with anti-B19 virus neutralizing antibody-positive, but not -negative human serum (data not shown). Collectively, these results indicate that B19 infection induced the unique B19-B population characterized by the "G2-arrested" phenotype.

B19 infection induces autophagosome-like vesicles

To further characterize the B19-B population, we next examined the permeability of mitochondria and plasma membranes in B19-infected cells, because we suspect that the FSC^{high} phenotype indicates the enlargement of cell size which is an outcome of the increase in cell membrane permeability. However, no significant difference was detected, suggesting that neither oncosis nor typical apoptosis mediates the B19-induced changes (data not shown). Because the high SSC in FACS analyses is likely to represent the higher 'complexity' within the cytoplasm, we then decided to directly examine the intracellular organization of cells from the B19-B population by electron microscopy (EM). On days 2 and 5 after the B19 infection, cells were fixed and subjected to the analyses. A remarkable difference in cell morphology was observed; most of the B19-infected cells were relatively larger with diameter of approximately 16–24 μm, whereas that of mock-transfected cells were only 8–9 μm (Figs. 2Aa, b, and c). The percentages of cells having diameters of more than 15 μm were 2.6 ± 1.2%, 48.7 ± 3.7% and 11.6 ± 3.0% in mock-infected, day two and day five of the B19 infection, respectively (Fig. 2B). Another significant difference observed in the infected cells on day 2 was the shape of their nuclei, which manifested lower EM density with swollen shape and ruffled nuclear membranes. In addition to the altered morphology of the nuclei, the size of the cytoplasm was quite enlarged. Of note, many EM-dense spherical structures were scattered among the cytoplasm. These membrane surrounded structures were observed more frequently in the larger sized than the normal-sized cells on day 2 after the infection (Fig. 2Ah). Some of the membrane surrounded structures seemed to contain degraded mitochondria with double membrane structure (Figs. 2Ah and k). Taking into account the 'vesicles' with double-membrane like

structure, we speculated that these organellas most resemble autophagosomes. Interestingly, the autophagosome like vesicles showed increase in their size from an average diameter of 0.2 μm to 0.6 μm on day 5 (Figs. 2Ai and l). Unlike the B19 infection, mock infection did not induce any of these changes (Figs. 2Ag and j). Furthermore, a significant percentage of

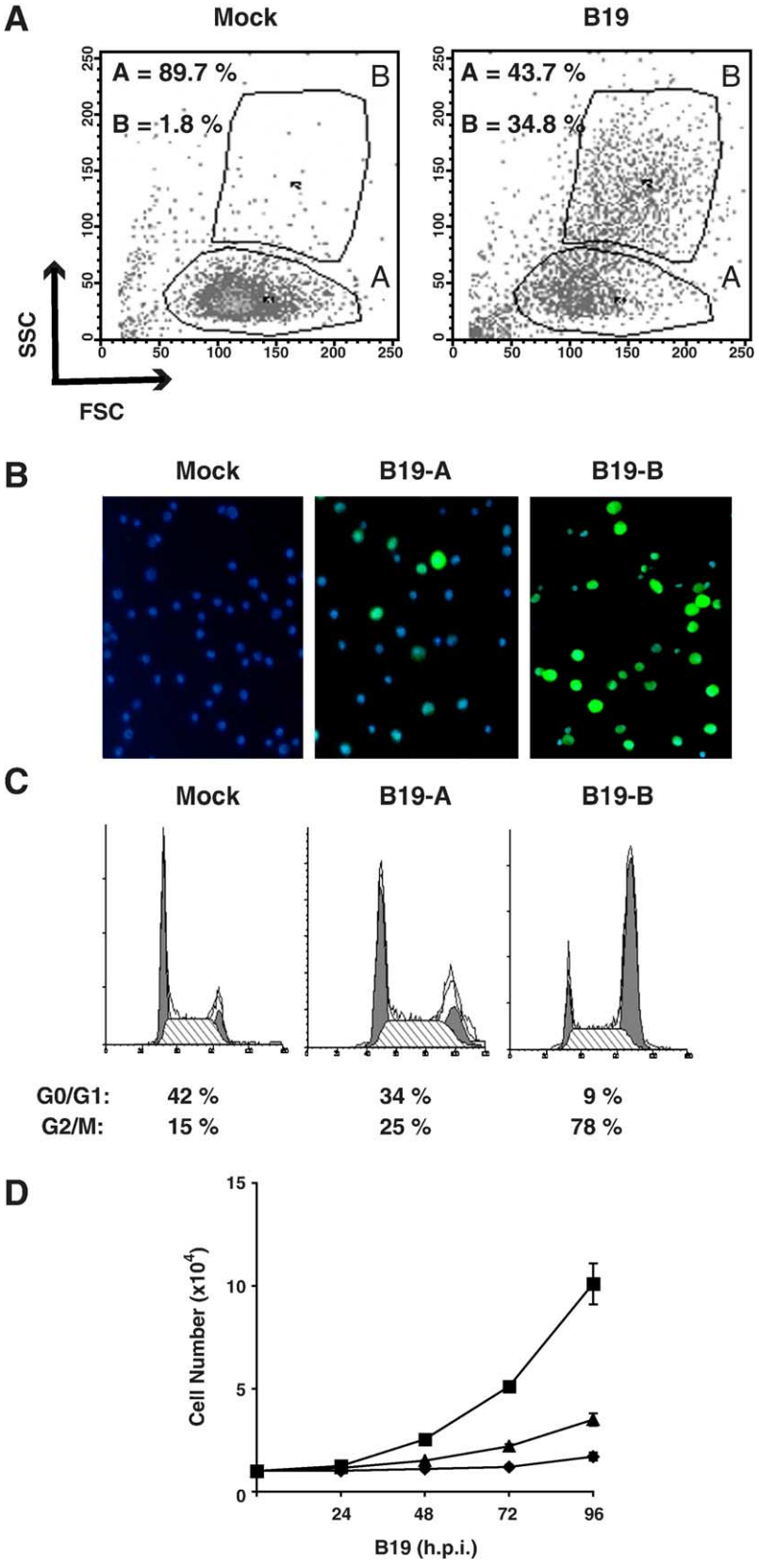

cells manifested shrunk morphology and higher EM density (Figs. 2Ac, arrows), suggesting an increase in cells with apoptotic phenotype on day 5 compared with negligible number of cells with similar phenotype on day 2 or mock-infected cells (Figs. 2Aa, b, and c). Therefore, both apoptotic and autophagic cells were detected on day 5 (Fig. 2Ai). Taken together, these results suggest that B19 infection induced not only smaller apoptotic cells but also enlarged cells carrying significant numbers of autophagosome-like vesicles.

Activation of autophagy in B19-infected cells

To further examine whether the autophagosome like vesicles frequently found within the B19-infected cells indeed represent activation of autophagy in these cells, we tested the expression of LC3, which specifically labels autophagosome and thus is a hallmark of autophagy. At quiescent status, LC-3 basically resides in the cytoplasm as a precursor form, LC3-I. However, upon exposure to various environmental stresses to provoke autophagy, it is rapidly degraded to produce a lipidated form, LC3-II, which then sticks onto autophagosomes. Therefore, the LC3-II/LC3-I ratio well correlates with the number of autophagosomes (Kabeya et al., 2000). We infected UT7/Epo-S1 cells with B19. Cell lysates prepared from cells at 96 h post-infection were subjected to Western blot analysis. We found time-dependent increase of the LC3-II/LC3-I ratio, which maximized at 96 h post-infection (Figs. 3A and B). Accordingly, expression of NS1 also maximized at the same 96 h post-infection (Fig. 3A).

To further clarify whether autophagy occurs in B19-infected cells, we next immunostained endogenous LC3 on fixed cells and analyzed by the immunofluorescence confocal microscopy. In the mock-transfected cells, LC3 was diffusely expressed under a non-starved condition (Fig. 3C). Upon B19 infection, however, LC3-positive larger dots that represent autophagosomes, were clearly identified mostly within the cytoplasm as judged by the simultaneous staining of NS1 protein, which resides within the nucleus. Noteworthy, LC3-positive autophagosomes were only detected in NS1-positive cells, but not in NS1-negative cells (Fig. 3C). These results indicate that B19-induces autophagy that maximizes at 96 h post-infection, with good accordance with NS1-expression.

B19-induced autophagy correlates with survival of infected cells

We next explored a biological significance of autophagy in B19-infected cells. To clarify whether abrogation of autophagosome formation has any effect on infected cells, we performed B19 infection experiments using UT7/Epo-S1 cells in the presence or absence of a specific autophagy inhibitor, 3-methyladenine (3-MA). At 48 h after the infection, 3-MA was added to the culture and further incubated for additional 24 h. To examine whether blockade of autophagy may alter the cell viability, cells in the sub-G1 fraction, which represent dead cells, were analyzed by a flow cytometry. Surprisingly, percentage of dead cells after the B19 infection showed significant increase in the presence of 3-MA; 27% and 12%, in the presence or absence of 3-MA, respectively (Fig. 4A). This increase in dead cells by the abrogation of autophagy is rather specific to B19 infection because mock-transfected cells conferred little if any alteration in the viability. On the other hand, 3-MA did not alter the NS1 expression, irrespective of B19 infection as judged by the immunocytochemical analyses suggesting similar B19 infection efficiency (data not shown). To further clarify the effect of autophagy inhibitor on B19-induced cell death, we determined to quantify the 'Autophagic Cell Death Index' (hereafter referred as ACD index), which is calculated by the ratio of dead cells in the presence and absence of 3-MA (3-MA(+)/3-MA(−)). This index is expected to represent effects of autophagy inhibitor on B19- or mock-infected cells. After the initial B19 infection period of 24, 48, 72, and 96 h, cells were cultured in the presence or absence of the 3-MA for additional 24 h, and the numbers of dead cells were determined. For a control, cells without infection (referred as "0 h" infection) were incubated in the presence or absence of 3-MA for 24 h. The ACD index on B19 infection showed 1.7-fold increase at 24 h after the infection, which maximized up to 2.5 at 48 h, whereas little if any effects of 3-MA on mock-infected cells (Fig. 4B). Finally, we examined the ACD index in a time-dependent manner by 3-MA treatment on cells at 48 h time point after the B19 infection (Fig. 4C). When B19-infected cells were used for this assay, the ACD index showed a modest increase at the initial 12-h time point after the 3-MA incubation and a maximum score was obtained at 24 h after the treatment. On the other hand, almost negligible increase was observed in the mock infection, suggesting little if any effect of 3-MA on cell death. Collectively, these results suggest that autophagy is involved in the survival of B19-infected cells which is most prominent at later stages of infection including 48 to 96 h after infection.

Discussion

In the present study, we provide the first evidence that cellular autophagy is induced by the human parvovirus B19. Autophagy induced in the B19-susceptible UT7/Epo-S1 cells is at least partially required for the infected cell survival.

In this study, we identified a novel cell population, B19-B, after B19 infection (Figs. 1A, B). This new population, because

Fig. 1. (A) Identification of a unique population in B19-infected cells (Upper panels). Flow cytometric analyses of UT7/Epo-S1 cells which were infected with B19 virus for 48 h. Cells were infected with B19 virus (right) and mock (left). The percentages of cell numbers in area A ($FSC^{high}SSC^{low}$) and B ($FSC^{high}SSC^{high}$) are shown. (B) Expression of NS1 in B19-infected cells. B19-infected cells were immunolabeled with anti-NS1 and FITC-conjugated anti-mouse IgG secondary antibody (green). Nuclei were detected by DNA staining with 4′,6′-diamidino-2-phenylindole (blue). (C) Cell cycle analysis of B19-infected populations. After segmentation, B19-infected or mock-infected cells were labelled with PI to detect DNA content and analyzed by FACS caliber. (D) Cell growth of B19 virus-infected-A, B and mock-infected UT7/Epo-S1 cells. UT7/Epo-S1 cells were infected with B19 virus and counted. Area A (triangles), area B (diamonds) of B19 infection or mock infection (squares) are indicated. Experimental data presented are representative of at least three experimental data with similar results.

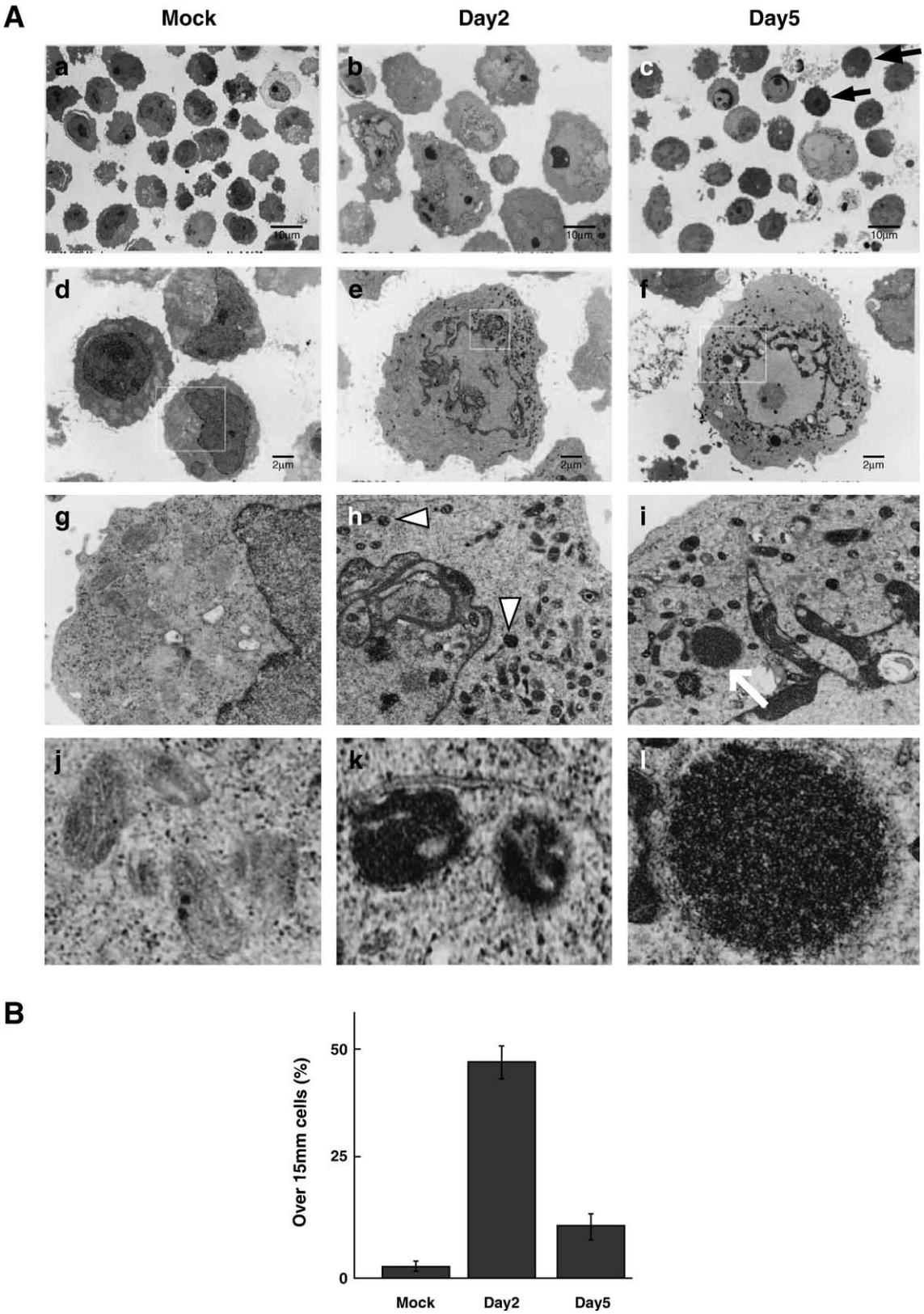

Fig. 2. Electron microscopy of B19 virus induced enlarged cells. UT7/Epo-S1 cells were infected with B19 virus, and fixed on days 2 (B), 5 (C). Mock-infected cells are used as control (A). Lower panels g–l respectively show the region outlined by white lines in above panels d–f. Black arrows indicate dying cells among the B19-infected cells (c). Open arrowheads indicate EM-dense mitochondria (h). White arrow (i) indicates EM-dense aggregates, possibly containing degraded mitochondria. Closed arrow heads (k) indicate the double-membrane structure. Mitochondria in mock infection (j), in B19 infection after day 2 (k) are also magnified. Scale bars, 10 μm (a–c), 2 μm (d–f) are indicated.

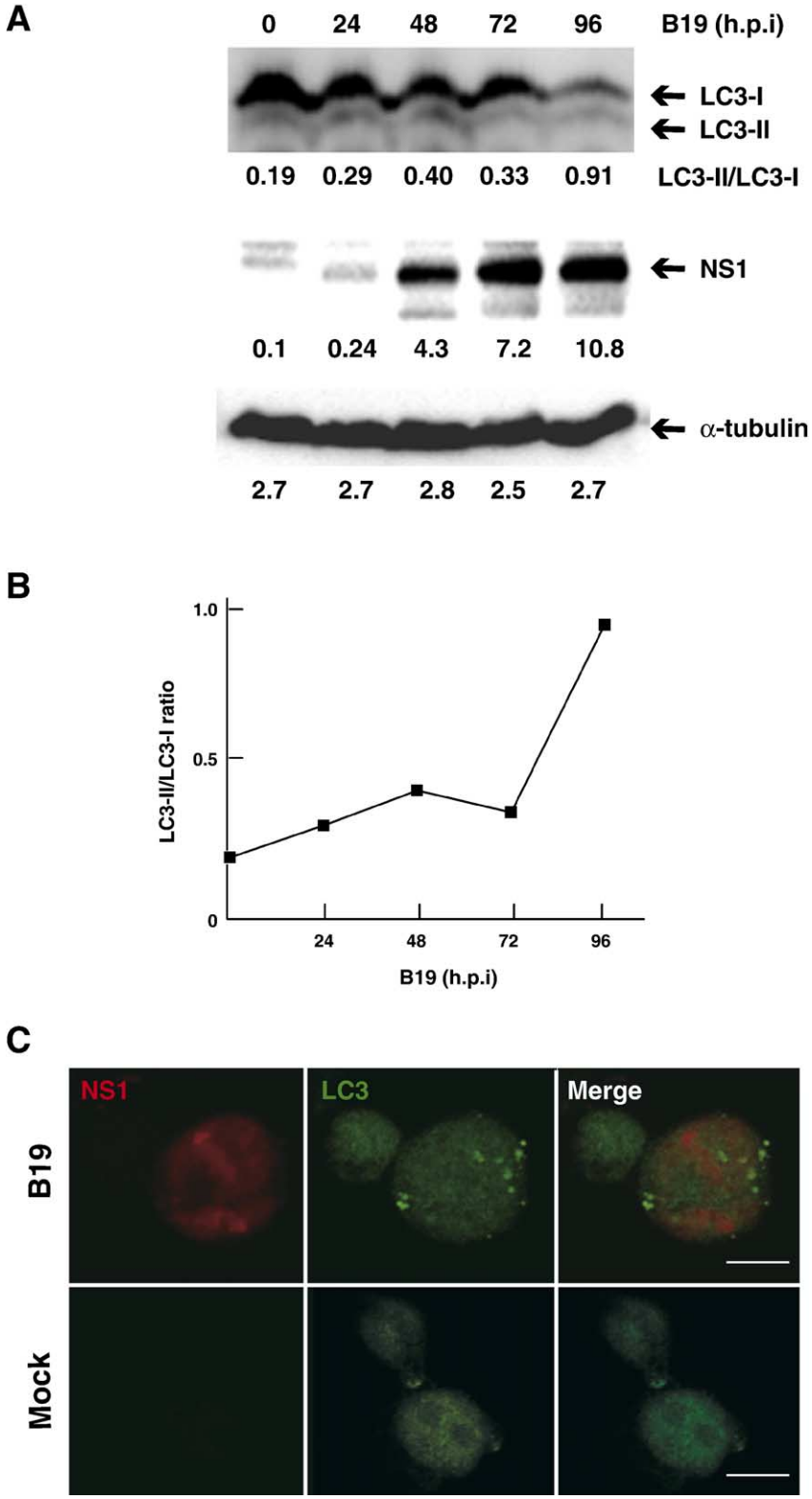

Fig. 3. Autophagy in B19-infected UT7/Epo-S1 cells. (A) Immunoblot analysis of LC3-II in cells infected with B19 virus at indicated times; 0, 24, 48, 72, and 96 h. The band intensities of endogenous LC3-I and LC3-II were quantified, and the LC3-II/LC3-I ratio is indicated. Band intensities for NS1 and α-tubulin are also shown. (B) The LC3-II/LC3-I ratio. Number calculated from panel A is shown. (C) Native LC3 expression in NS1-expressing cell. UT7/Epo-S1 cells were infected. B19 virus- or mock-infected cells were fixed and subjected to confocal microscopy analysis; NS1 staining (left panels), LC3 staining (middle panels) and merged images (right panels) of the same field are shown. Scale bars: 10 μm.

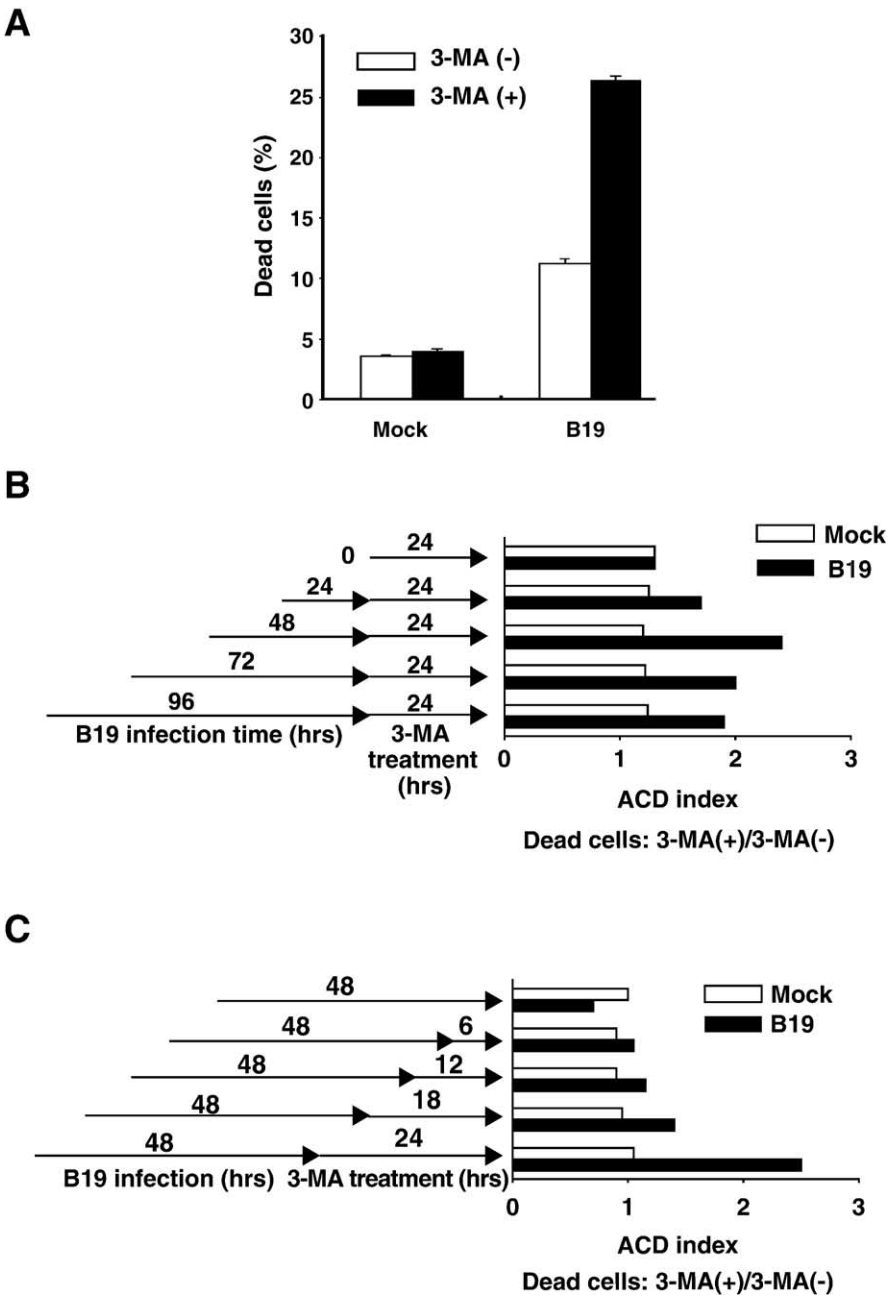

Fig. 4. The inhibitor of autophagy induces cell death in B19-infected cells. The percentages of dead cells were calculated with sub-G1 populations. (A) The percentage of dead cells treated with DMSO (open bars) or 5 mM 3-MA (solid bars) after 72 h post-infection. After the initial B19 infection for 48 h, cells were incubated in the presence of DMSO or 3-MA for additional 24 h. (B and C) UT7/Epo-S1 cells were infected with B19 virus (triangle) or mock (square). *Y*-axis indicates the ACD index, which is calculated by the ratio of dead cells in the presence and absence of 3-MA (3-MA(+)/3-MA(−)). (B) Kinetic analyses of ACD index on B19- or mock-infected cells. Cells were initially incubated in the presence or absence of B19 for 24, 48, 72, or 96 h, extensively washed, and then further incubated with or without 3-MA for 24 h. ACD index at the time point 0 was obtained from cells without infection and incubated with or without 3-MA for 24 h. (C) Kinetic analyses of ACD index on cells initially infected with B19 for 48 h. After the initial 48 h infection periods, cells were washed extensively and then cultured in the presence of 3-MA for indicated times on *X*-axis. Each experimental data represent from at least three independent experiments.

of its larger size and higher intracellular complexity, may be at least similar to the "cytopathic giant pronormoblasts" which appears among the B19 parvovirus inoculated normal bone marrow cells at 48 h after infection (Ozawa et al., 1987). Since no additional characteristics of the cytopathic giant pronormoblasts have been analyzed before, we could not fully distinguish the giant pronormoblasts found in bone marrow cells and the B19-B population in the UT7/Epo-S1 cells in the present study.

One interesting characteristics we found regarding the B19-B population is a profound G2-arrest phenotype (Fig. 1C). Cell cycle arrest status of B19-B was not only obvious by the FACS analysis but also evident in their severely retarded cell growth (Fig. 1D). Therefore, these B19-B cells are in good accordance with our former observation that B19 infection mediates cell cycle arrest at G2 phase with decreased cell viability (Morita et al., 2001).

We found that the cells from the B19-B population manifest significant morphological alternation compared with mock-infected cells (Figs. 2A, B). The swollen change was clearly identified in B19-infected cells and therefore can be interpreted as cytopathic effect. Although we formerly reported that B19 induces apoptosis (Yaegashi et al., 1999), cell enlargement is usually atypical. Since cell fate of the B19-B population should be either apoptosis or survival, we tested the former possibility. We found no characteristic observation found in apoptotic or necrotic cells, as judged by the permeability of mitochondria or plasma membrane (data not shown). We therefore conclude that the morphological alternation we found in the B19-B cells may be associated with their G2-arrest phenotype.

To our surprise, our EM analyses clearly revealed morphological characteristics within the cytoplasm. Organellas within the B19-infected enlarged cells, both on days 2 and 5, contained mitochondria which were at least partially degraded (Figs. 2Ah–l). Similar intracellular structures have been reported in sympathetic neurons after nerve growth factor (NGF) withdrawal (Kirkland et al., 2002). Mitochondria with EM-dark matrix have been interpreted as "matrix condensation", which have almost lost their proper definition, therefore appear as single-membrane structure containing EM-dense materials. We believe that our present study is the first report stating mitochondrial degeneration in B19-infected cells. In addition, it is of great interest that elimination of mitochondria is now shown to be at least partially mediated by cellular autophagy (Kissova et al., 2004). Further, a previous study demonstrated a coincidence between the onset of mitochondrial shrinkage (but not swelling) and the engulfment of mitochondria by autophagosomes (Tolkovsky et al., 2002). In this study, we clearly found that the degrading mitochondria were sequestrated by a double membrane structure, which is a hallmark of autophagosomes (Fig. 2Ak). To our knowledge, this study first reports the DNA virus-induced autophagy. Taken together with this notion, we conclude that B19-induced enlarged cells are actively engulfing mitochondria by way of cellular autophagy.

We also confirmed the induction of autophagy by biochemical analyses in B19-infected cells. Conversion of LC3, from cytoplasmic precursor LC3-I to lapidated and therefore autophagosomal resident LC3-II form, was clearly identified not only by Western blots but also by confocal microscopy (Figs. 3A and C). One characteristic feature of B19-induced autophagy is its appearance in the later time point after the infection, which seems to be the most at 48 to 96 h time points (Fig. 4B). This kinetics should be quite different from autophagy induced by nutrient starvation or the group A Streptococcus (GAS) infection, both of which are most apparent at least 3 to 6 h after the induction (Yoshimori, 2004). One explanation for the relatively late onset of autophagy is that some de novo synthesized viral protein may induce autophagy, while it may just be induced by general increase of cellular stress. To explore the former possibility, we tested whether NS1 induces autophagy, because NS1 expression seems to somewhat proceed the induction of autophagy (Figs. 3A and B). At present, however, we have obtained marginal induction of autophagy by NS1. We need to identify a mechanism by which B19 induces autophagy, such as other viral protein or cellular innate response against B19 infection.

Our present study demonstrated that autophagy induced by B19 mediates infected cell survival (Fig. 4A). At present, however, we do not have direct evidence for the precise biological significance of autophagy in B19-infected cells. One possibility is that infected cells inhibit B19 virus by sequestration the viral component, while another is that cells survive by mitochondrial breakdown and nutrient supply. NS1-expressed cells might result either from the use for virus replication or the destruction of the virus structure. In this context, it is interesting to see how other virus utilize autophagy. In RNA virus infection, such as poliovirus, RNA replication complexes co-localize with autophagosomes and thereby utilize the autophagic machinery for the virus replication. In the case of murine hepatitis virus (MHV), a member of the Coronaviridae, requires the autophagic pathway to form infectious virions, since the yield of extracellular virus is significantly diminished in clonal isolates of Atg5$^{-/-}$ mouse embryonic stem cells (Kirkegaard et al., 2004). Considering these RNA virus tactics to utilize the autophagy machineries, we speculate that B19 also may use autophagy for their propagation. If this hypothesis is correct, B19-infected cells treated with 3-MA may survive longer than non-treated cells, because B19 has an ability to induce apoptosis. Nevertheless, we found an opposite effect, indicating that autophagy rather facilitated cell survival. Regarding the B19-infected cell fate, we previously reported a typical kinetics, in which most of the infected cells get arrested at G2 phase within 12 h after the infection, then survive up to 72 h, and start dying accompanied with viral replication (Morita and Sugamura, 2002). In this study, we showed that inhibition of autophagy is most effective at 48 to 72 h after the infection, and thereafter decreases. Thus, autophagy seems to work during the initial 48–72 h after the B19 infection, probably in cells arrested at G2 phase, before they are competent for the virus replication. We speculate that whereas some enlarged cells fall into apoptosis following the G2-arrest, other enlarged ones manage to survive by activating the autophagy machinery. In other words, autophagy may benefit B19 allowing their expansion during the "time lag". To verify the hypothesis, we must overcome at least two major barriers. One is that, as far as we know, cell lines that are highly susceptible to B19 are limited. Second, little is known regarding the B19 expansion, from replication to release. To solve these problems, we need a cell line, which is highly propagative as well as highly susceptible to B19 infection.

Collectively, we first demonstrated that DNA virus infection induces autophagy. Autophagy induced by B19 contributed to cell survival, potentially leaving time periods for the viral replication and expansion. Further experiments are needed to explore the "fight" between the B19 and the host.

Material and methods

Cell line and chemicals

B19 virus antigen-positive human serum obtained from a blood donor was used as a B19 virus seed, the virus titer of

which was calculated to be 10^8 infectious units per milliliter by anti-VP1/2 immunostaining assays. UT7/Epo-S1 cells were inoculated with a multiplicity of infection of 10 with 20-fold-diluted virus seed at 10^6 cells/ml in Isocove's modified Dulbecco's medium (IMDM) and incubated for 2 h at 4 °C for virus adsorption. UT7/Epo-S1 cells, highly susceptible to B19 virus infection (Morita et al., 2001), were propagated in Isocove's modified Dulbecco's medium containing 10% fetal calf serum and 2 U/ml recombinant erythropoietin (Epo) (a gift from Kirin Brewery Pharmaceutical Research Laboratory, Tokyo, Japan). 3-Methyladenine (3-MA) was obtained from Sigma-Aldrich (Steinheim, Germany) and dissolved directly to the incubation medium.

Flow cytometry analysis

Cells were harvested, washed once and then resuspended in PBS solution containing 5 μg/ml propidium iodide (PI) and incubated at 37 °C for 30 min. Samples were then analyzed with a FACS Calibur flow cytometer using the Cell Quest software (BD Biosciences, Mountain View, CA).

Cell cycle analysis

Cell cycle analyses were performed as described previously (Darzynkiewicz et al., 1992). In brief, cells were infected with B19 virus and cultured for the indicated times. After the cells were washed twice with phosphate-buffered saline (PBS), they were suspended in propidium iodide (PI) solution (50 μg/ml PI, 0.1% sodium citrate, 0.2% NP-40, 0.05 mg/ml RNase), then incubated for 30 min at 4 °C. Cells in the sub-G1, G_0/G_1 and G_2/M fractions were counted with a FACScan fluorescence-activated cell sorter (FACS; BD Bioscience, Franklin Lakes, NJ). For some experiments, cells were infected with B19 for 24, 48, 72, or 96 h, and then washed with PBS three times. Subsequently, cells were further incubated with 5 mM 3-MA at 37 °C for additional 24 h. Dead cells including apoptosis were analyzed by flow cytometry, by determining the cells within sub-G1 fraction.

Western blotting

Whole-cell lysates were prepared with a lysis buffer (2% NP-40, 0.2% SDS in PBS supplemented with protease inhibitors). Western blot analyses were carried out as described previously (Nakashima et al., 2004). Anti-NS1 monoclonal antibody (MAb), ParC-NS1, specific for the NS1 C-terminal half of B19 virus (Morita et al., 2003), and anti-LC3 antibody against recombinant LC3 (Kabeya et al., 2000) were previously described. Anti-α-tubulin MAb (Sigma Aldrich Fine Chemicals, St. Louis, MO) was also purchased.

Electron microscopy

Cells were mock-infected, infected for 2 day or 5 day, and then washed once with 0.1 M cacodylate buffer, pH7.4. The cells were fixed with 2% glutaraldehyde in 0.1 M phosphate buffer. Subsequently, the rests of the procedure were conducted by Nissin EM Corp (Tokyo, Japan).

Immunocytochemistry

Immunocytochemistry was carried out as described previously (Morita et al., 2001). In brief, cells were fixed in 4% paraformaldehyde (PFA)–PBS for 15 min and labeled with following antibodies; anti-NS1 MAb antibody and anti-LC3 antibody. They were secondarily stained with Alexa Fluor 488 goat anti-mouse antibody and Alexa Fluor 594 goat anti-rabbit antibody (Molecular Probes, Inc., Eugene, OR). Confocal images of fluorescent materials in UT7/Epo-S1 cells were collected using a confocal laser scanning microscope, LSM510 META (Carl Zeiss, Oberkochen, Germany).

Acknowledgments

We gratefully acknowledge the gift of recombinant Epo from Kirin Brewery Pharmaceutical Research Laboratory, Tokyo, Japan. The authors thank Mr. Lamichhane Aayam for critically reading the manuscript. This work was supported in part by a Grant-in-aid for Scientific Research from the Japan Society for the Promotion of Science (JSPS), the 21st century Center of Excellence (COE) Program and Grant-in-aids for Scientific Research on Priority Areas from the Ministry of Education, Science, Sports, and Culture, a Grant-in-aid from the Ministry of Health, Labor, and Welfare of the Japanese Government. K.T. and M.K. are JSPS research fellows.

References

Darzynkiewicz, Z., Bruno, S., Del Bino, G., Gorczyca, W., Hotz, M.A., Lassota, P., Traganos, F., 1992. Features of apoptotic cells measured by flow cytometry. Cytometry 13 (8), 795–808.

Kabeya, Y., Mizushima, N., Ueno, T., Yamamoto, A., Kirisako, T., Noda, T., Kominami, E., Ohsumi, Y., Yoshimori, T., 2000. LC3, a mammalian homologue of yeast Apg8p, is localized in autophagosome membranes after processing. EMBO J. 19 (21), 5720–5728.

Kirisako, T., Ichimura, Y., Okada, H., Kabeya, Y., Mizushima, N., Yoshimori, T., Ohsumi, M., Takao, T., Noda, T., Ohsumi, Y., 2000. The reversible modification regulates the membrane-binding state of Apg8/Aut7 essential for autophagy and the cytoplasm to vacuole targeting pathway. J. Cell Biol. 151 (2), 263–276.

Kirkegaard, K., Taylor, M.P., Jackson, W.T., 2004. Cellular autophagy: surrender, avoidance and subversion by microorganisms. Nat. Rev., Microbiol. 2 (4), 301–314.

Kirkland, R.A., Adibhatla, R.M., Hatcher, J.F., Franklin, J.L., 2002. Loss of cardiolipin and mitochondria during programmed neuronal death: evidence of a role for lipid peroxidation and autophagy. Neuroscience 115 (2), 587–602.

Kissova, I., Deffieu, M., Manon, S., Camougrand, N., 2004. Uth1p is involved in the autophagic degradation of mitochondria. J. Biol. Chem. 279 (37), 39068–39074.

Morita, E., Sugamura, K., 2002. Human parvovirus B19-induced cell cycle arrest and apoptosis. Springer Semin. Immunopathol. 24 (2), 187–199.

Morita, E., Tada, K., Chisaka, H., Asao, H., Sato, H., Yaegashi, N., Sugamura, K., 2001. Human parvovirus B19 induces cell cycle arrest at G (2) phase with accumulation of mitotic cyclins. J. Virol. 75 (16), 7555–7563.

Morita, E., Nakashima, A., Asao, H., Sato, H., Sugamura, K., 2003. Human parvovirus B19 nonstructural protein (NS1) induces cell cycle arrest at G (1) phase. J. Virol. 77 (5), 2915–2921.

Nakagawa, I., Amano, A., Mizushima, N., Yamamoto, A., Yamaguchi, H., Kamimoto, T., Nara, A., Funao, J., Nakata, M., Tsuda, K., Hamada, S., Yoshimori, T., 2004. Autophagy defends cells against invading group A Streptococcus. Science 306 (5698), 1037–1040.

Nakashima, A., Morita, E., Saito, S., Sugamura, K., 2004. Human Parvovirus B19 nonstructural protein transactivates the p21/WAF1 through Sp1. Virology 329 (2), 493–504.

Ozawa, K., Kurtzman, G., Young, N., 1987. Productive infection by B19 parvovirus of human erythroid bone marrow cells in vitro. Blood 70 (2), 384–391.

Tolkovsky, A.M., Xue, L., Fletcher, G.C., Borutaite, V., 2002. Mitochondrial disappearance from cells: a clue to the role of autophagy in programmed cell death and disease? Biochimie 84 (2–3), 233–240.

Yaegashi, N., Niinuma, T., Chisaka, H., Uehara, S., Moffatt, S., Tada, K., Iwabuchi, M., Matsunaga, Y., Nakayama, M., Yutani, C., Osamura, Y., Hirayama, E., Okamura, K., Sugamura, K., Yajima, A., 1999. Parvovirus B19 infection induces apoptosis of erythroid cells in vitro and in vivo. J. Infect. 39 (1), 68–76.

Yoshimori, T., 2004. Autophagy: a regulated bulk degradation process inside cells. Biochem. Biophys. Res. Commun. 313 (2), 453–458.

Young, N., Harrison, M., Moore, J., Mortimer, P., Humphries, R.K., 1984. Direct demonstration of the human parvovirus in erythroid progenitor cells infected in vitro. J. Clin. Invest. 74 (6), 2024–2032.

Yu, L., Alva, A., Su, H., Dutt, P., Freundt, E., Welsh, S., Baehrecke, E.H., Lenardo, M.J., 2004. Regulation of an ATG7-beclin 1 program of autophagic cell death by caspase-8. Science 304 (5676), 1500–1502.